Nanoscale

PAPER

Cite this: *Nanoscale*, 2015, **7**, 7065

Additive-free thick graphene film as an anode material for flexible lithium-ion batteries†

Kuldeep Rana, Seong Dae Kim and Jong-Hyun Ahn*

Received 15th October 2014,
Accepted 15th December 2014

DOI: 10.1039/c4nr06082b

www.rsc.org/nanoscale

This work demonstrates a simple route to develop mechanically flexible electrodes for Li-ion batteries (LIBs) that are usable as lightweight effective conducting networks for both cathodes and anodes. Removing electrochemically dead elements, such as binders, conducting agents and metallic current collectors, from the battery components will allow remarkable progress in this area. To investigate the feasibility of using thick, additive-free graphene films as anodes for flexible LIBs, we have synthesized and tested thick, additive-free, freestanding graphene films as anodes, first in a coin cell and further in a flexible full cell. As an anode material in a half cell, it showed a discharge capacity of about 350 mA h g^{-1} and maintained nearly this capacity over 50 cycles at various current rates. This film was also tested as an anode material in a full cell with a $LiCoO_2$ cathode and showed good electrochemical performance. Because the graphene-based flexible film showed good performance in half- and full coin cells, we used this film as a flexible anode for flexible LIBs. No conducting agent or binder was used in the anode side, which helped in realizing the flexible LIBs. Using this, we demonstrate a thin, lightweight and flexible lithium ion battery with good electrochemical performance in both its flat and bent states.

1. Introduction

There is an increasing demand for lightweight, higher-capacity, low-cost, more stable and safe rechargeable batteries to meet special needs for next-generation high-performance portable electronic devices and electric vehicles.[1–6] Synthetic and natural graphite have been generally used as anode materials of commercial LIBs. Recently, carbon nanostructured materials such as carbon nanotubes (CNTs) and graphene have been evaluated as promising materials to improve the performance of electrodes due to their excellent electrical properties and their higher capacity compared to that of graphite[7,8] However, current research has also focused on flexible and wearable electronic devices such as roll-up display, light-emitting diodes, and smart watch.[9,10] Such devices are being developed rapidly and essentially require flexible rechargeable batteries to achieve all-in-one flexible systems. Fabrication of flexible LIBs requires flexible electrodes, separators and substrates. Generally, traditional electrodes used in LIBs are composed of mixtures of active materials, binders and conductive carbon additives, such as carbon black, graphite and CNTs, which are coated over metal current collectors of copper (10 mg cm^{-2}) and aluminum (5 mg cm^{-2}). Additives and the metal current collector, being electrochemically inactive, reduce the overall energy density and add extra weight to the battery. Thus, the ability to remove such additives and produce an additive-free, flexible electrode would represent remarkable progress for high-performance flexible LIBs. A flexible electrode could be either an active material with intrinsic flexibility, or a composite electrode based on a flexible substrate. A number of research reports have discussed the possibility of using flexible electrodes based on CNTs to replace heavy metals.[11,12] CNT paper, which can be prepared by various methods,[13–18] can be used as both a flexible electrode and a current collector due to its light weight and good interface as a current collector, with low sheet resistance of ~5 Ω sq^{-1} and light weight of ~0.2 mg cm^{-2} compared to metal current collectors.[6] Recently, graphene and its derivatives have attracted interest as electrode materials for supercapacitors[19] and LIBs[20] due to their high electrical conductivity, large surface area, fast-reacting edges, high lithium diffusivity, superior mechanical flexibility and low cost.[21] Moreover, lightweight graphene foam has recently been used as a current collector for flexible LIBs using traditional electrodes. Recently, our group has used thick freestanding graphene paper as a current collector, using MoS_2 as an anode material.[22]

A number of efforts to develop flexible LIBs have been made by using various types of flexible electrodes; however, this research area still remains in the early stages of development. Most of the electrodes reported in flexible LIBs have used additives such as polymeric binder and carbon black,

School of Electrical and Electronic Engineering, Yonsei University, Seoul, 120-749, Korea. E-mail: ahnj@yonsei.ac.kr

†Electronic supplementary information (ESI) available. See DOI: 10.1039/c4nr06082b

and have also used metallic current collectors.[6] These elements are not suitable for flexibility and have other drawbacks, as mentioned above. In this work we report a simple synthesis process to prepare thick, flexible, freestanding graphene paper by a chemical vapor deposition (CVD) method. Our aim is to use this flexible paper as an anode material in LIB and, which simultaneously works as a current collector. This thick, flexible graphene paper showed excellent mechanical flexibility and could be bent into any desired structure. In this work, we did not include any additives, minimizing the dead cell components that are electrochemically inactive and also reduces the number of production steps. There was no significant difference in the electrochemical performance of the flexible LIBs in their bent and flat states, indicating good mechanical flexibility. Most graphene-based flexible devices that have previously been reported are based on chemically converted graphene containing many impurities or have used additives that do not contribute to electrochemical performance and are not helpful in producing flexibility of LIB. Thus the thick freestanding graphene in our study is suitable for an electrode, as well as current collector for flexible LIB and can be directly used for LIB testing without a binder or current collector. This novel structure exhibits good electrochemical properties and mechanical flexibility in flexible LIBs.

2. Experimental section

Thick graphene films were grown on Ni metal foil substrates 25 μm thick using a thermal CVD process. The substrates were first placed away from the heating zone of a tubular furnace and the temperature was raised to 1000 °C and a steady flow of argon was supplied with the flow rate of 100 sccm. The polycrystalline Ni substrates were loaded into the center of the tube furnace after the temperature reached 1000 °C, and simultaneously hydrogen with a flow rate of 150 sccm was allowed to flow. Graphene growth was started by means of decomposition of methane by flowing 400 sccm of methane and keeping 150 sccm of hydrogen in the furnace for 4 h. The carbon source decomposed, dissolving and diffusing into the nickel layer; subsequently, upon fast cooling, the carbon segregated on both sides of the nickel to form a thick graphene film. To delaminate graphene film, Ni was etched away by a $FeCl_3$-based etchant, and a thick freestanding graphene (FSG) film was obtained. X-ray diffraction (XRD) analysis was performed using an X-ray diffractometer with monochromatized CuKα radiation (λ = 0.15405 nm). Various vibration modes were obtained using a Raman spectrometer having 532 nm lasers operated at 10 mW power. Field emission scanning electron microscopy was used to study the surface morphology of the samples. Further investigations were carried out using X-ray photoelectron spectroscopy (XPS) to study the binding energies of various elements present in the CVD-grown thick graphene before and after cell testing.

Electrochemical testing was carried out using a coin half-cell fabricated in the configuration of Li/separator/FSG or Li/separator/G on Ni (*i.e.*, without or with Ni). The full coin cells have also been fabricated using a $LiCoO_2$ cathode with two different anodes (FSG and G on Ni). Finally flexible LIBs were fabricated using plastic (PET) substrates with thermally deposited aluminum (400 nm thick), which was used as cathode current collector. The cathode ($LiCoO_2$) material was finally coated on Al-deposited PET film. Both cathode and anode separated with polypropylene film were sealed with PET coverage. Electrolyte (1 mol L^{-1} $LiPF_6$ mixed with ethylene carbonate and di-ethyl carbonate 1 : 1 by volume) was injected in the flexible LIB in an argon-filled glove box with oxygen and moisture levels less than 1 ppm. Li metal foil was used as the counter electrode in the half coin cells. Polypropylene film was used as a separator between the electrodes, acting as an insulator for electrons but allowing lithium ions to diffuse through it. Cyclic voltammograms were obtained by measuring current–voltage response at the scan rate of 0.5 mV s^{-1} within the voltage range from 0.01 to 2.0 V. Electrochemical charge/discharge was performed in galvanostatic mode at the two different current densities of 50 and 150 mA g^{-1} for a number of charge/discharge cycles. All electrochemical measurements were carried out at room temperature.

3. Results and discussion

Fig. 1a shows the schematic illustration of a flexible lithium ion cell using a free-standing, additive free, thick graphene film (Using the thick graphene film as an anode, a thin film of $LiCoO_2$ as cathode was coated over an Al current collector, which was deposited over the PET film. Both were separated by

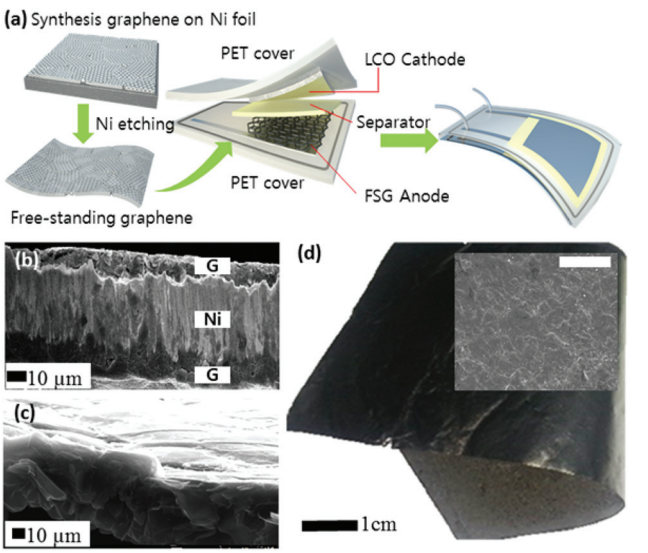

Fig. 1 (a) Schematic processes show the fabrication of a flexible lithium ion battery using a flexible electrode with PET covering; (b) SEM image shows the cross-sectional view of graphene film grown on both sides of Ni-film; (c) cross sectional view of FSG film after Ni etching; (d) the camera picture of FSG after Ni etching that is used directly as a flexible anode and the inset shows the surface morphology of thick graphene film (with scale bar 40 μm).

polypropylene film, and finally, the electrolyte was injected after sealing the cell inside the glove). First, the thick graphene film was grown over Ni films by CVD at 1000 °C.

However, most reports of CVD graphene growth on Ni have indicated the formation of mono- and few-layer graphene; our goal was to grow a very thick layer of graphene. The thickness and the number of graphene layers grown on Ni can be tuned by controlling parameters such as growth time, carbon concentration and cooling rate.[23] After the thick graphene film was grown over the Ni film, an optical image confirmed that the graphene had grown uniformly over the both side of Ni surface, as shown in the optical image (Fig. S1b†). The growth of graphene over Ni is one of the best examples of a strongly interacting interface due to hybridization of metal d-electrons with the π-orbital of graphene. Ni film acts as a catalyst that dissolves a large quantity of carbon (2.03 at%) atoms in its bulk and also precipitates a large amount of carbon on its surface upon rapid cooling, thus helping in the formation of many-layered graphene,[24] as shown in Fig. 1b. It is supposed that carbon atoms penetrate through the crack of the thick graphene layer grown on Ni and continuously grow graphene in the Ni catalyst layer, which results in thick graphite-like film with thickness in μm. The scanning electron microscope (SEM) image of a cross section of graphene film on Ni and after removing Ni is shown in Fig. 1b & c, respectively. The thick graphite-like film has been grown uniformly on both sides of the Ni film, and the thickness was estimated to be around 5–8 μm (Fig. 1b & c). After removing the Ni by etching, the cross section of FSG is also shown in Fig. 1c, which indicates that the many layers of graphene are stacked. The picture of freestanding graphene after Ni-etching is shown in Fig. 1d, which is easy in handling and can be used directly as an electrode without any post-treatment. The freestanding graphite-like films exhibit good mechanical flexibility, and their surface looks like patchwork, having sizes ranging from 5 to 15 μm, which provide the path for Li ion insertion into the graphene layers (inset of Fig. 1d). The optical and SEM images confirmed the uniformity of graphene film growth all over the surface of the Ni film. To understand the thick graphene film's crystallinity and to identify the chemical bonding present, detailed XRD, Raman spectroscopy and XPS characterizations were carried out. The XRD pattern of FSG after Ni-etching is shown in Fig. S2,† which shows the pure 2*H*-graphitic crystal structure without any remaining impurities of Ni. Using Raman spectroscopy (with an excitation wavelength 514 nm), we characterized the quality and nature of the thick graphene films; in the films spectrograms, two prominent peaks were observed: one at 1580 cm^{-1}, corresponding to the G-band which arising from in-plane vibrations of carbon atoms, and other at 2697 cm^{-1}, corresponding to the 2D-band and arising from a second-order Raman process. The G-band and 2D-band peaks had the line widths of 25 and 68 cm^{-1}, respectively (Fig. 2a). These very intense peaks in the Raman spectra confirm that Ni acts as a catalyst to induce the formation of well-formed crystalline carbon film by the volatile residual hydrocarbons. In addition, a low-intensity peak at

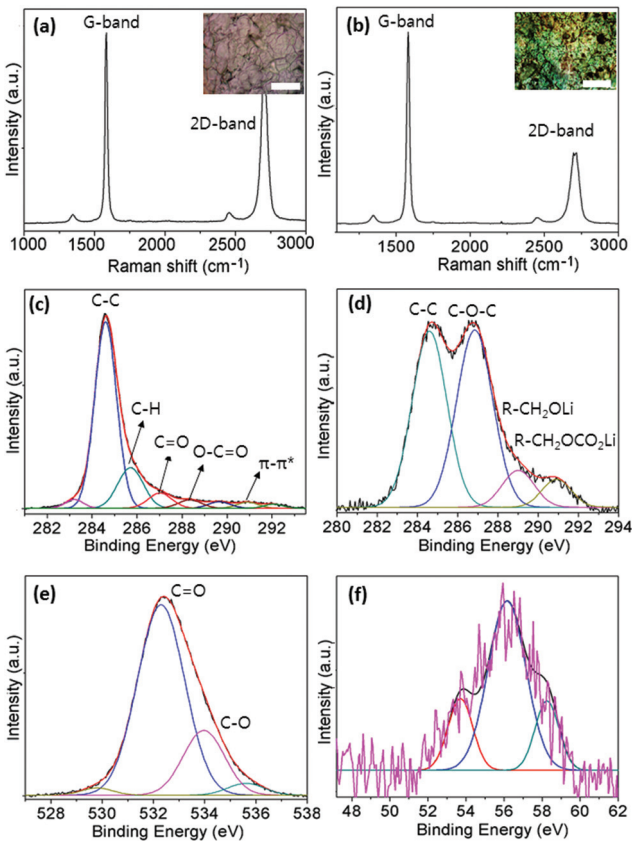

Fig. 2 Raman spectra of thick graphene grown over Ni-foil (a) before and (b) after cell testing; the inset shows the optical images from where spectra have been taken (with scale bar 10 μm). XPS spectra of thick graphene grown over Ni-foil (c) C1s peak of pure graphene (d, e & f) C1s, O1s and Li1s peaks after cell testing for the 50th cycle.

1347 cm^{-1} also appeared, suggesting a non-insignificant number of defects or disorder. These small amount of defects may arise due to the fast cooling, as a number of carbon atoms would not have enough time to reach a state of good crystallinity.[23] The I_D/I_G ratio was found to be 0.24, indicating that graphene film is well-formed crystalline than that obtained in a previous report.[23] In a Raman spectrum of a thick graphene film after cell testing, the G and 2D bands appeared at 1582 and 2704 cm^{-1}, respectively, with the respective line widths of 22 and 63 cm^{-1} (Fig. 2b). The G and 2D bands were at nearly the same positions as in the as-prepared films; however, the small shift observed in the 2D band was related to charge transfer, due to lithium intercalation in the carbon lattice. The intensity of the D-band was reduced after the cell test, which was attributed to the saturation of defects on the surface due to the formation of the solid electrolyte interphase (SEI), which saturates the defects on the surface due to the formation of various compounds. The chemical states of carbon atoms and chemical impurities, if any, were investigated by XPS before and after cell testing, and the acquired spectra are shown in Fig. 2c–f. Fig. 2c shows the C1s core-level XPS spectrum, which was dominated by a single peak at 284.5 eV, assigned to the sp^2 carbon network; support-

ing the Raman data (Fig. 1a), this confirmed again the good quality (defect free) of the graphene grown on Ni. However, at the bottom of the main line, toward its high-binding-energy side, a few other very low intensity peaks could be observed. These peaks are dependent on the chemical environment experienced by carbon atoms present on the surface, and thus correspond to the C1s components of different carbon groups.[25] Deconvolution showed that C–H bonded groups in a sp^3-hybridized state were present on the surface, as well as carbon–oxygen bonded groups of C═O and O═C–O. A deconvoluted XPS spectrum of C1s after cell testing showed two distinct peaks (Fig. 2d). The C1s signal from the graphene layer showed a small shift of 0.25 eV after cell testing; this small shift was attributed to the intercalation of lithium ions. The other peaks observed in the spectrum arose from various organic species deposited on the surface due to formation of the SEI during the first cycle; the corresponding XPS spectrum of oxygen is shown in Fig. 2e. The Li O1s spectrum after cell testing showed a major peak at around 56.2 eV, corresponding to Li_2O; this was because, after the cell anode was broken and thus exposed to oxygen, most of the lithium converted to Li_2O.[26] However, a small shoulder peak at 53.2 eV was present and assigned to lithium intercalation of the graphene film. After synthesis and characterization of the thick graphene film, it can be used directly as an anode material without requiring any post-treatment or additives. This additive-free thick graphene film has been used directly as an anode in half and full coin cells and also used in flexible LIB.

The electrochemical performance of the synthesized film (with or without Ni substrate) was firstly investigated in a coin half-cell, because its performance as an anode needed to be confirmed first in both a half and full cell to realize its application for flexible cells. The reversibility and kinetics of Li intercalation in the thick graphene film were studied using cyclic voltammetry. A cyclic voltammogram of a coin cell was obtained using a voltage sweep from 2.0 to 0 V *versus* a Li/Li^+ reference electrode at a scan rate of 0.5 mV s^{-1}; this demonstrated the reversible intercalation and de-intercalation of lithium into the carbon host (Fig. 3a). The lithium insertion potential was very low, close to 0 V *versus* Li/Li^+ reference electrode, whereas the potential for de-intercalation was around 0.4 V. The slight hysteresis observed in lithium intercalation and de-intercalation is a phenomenon that has been well discussed previously in carbonaceous materials.[27] In a five-cycle cyclic voltammogram of graphene film as an anode taken *versus* a Li/Li^+ reference electrode, the intensity of the redox peaks remained almost same in sequential cycles, indicating that the reversible Li insertion capacity was fairly stable for a number of cycles. This indicated that the binder-free and carbon-black-free electrode with good electrochemical behavior could serve as a very stable anode material for LIBs. A charge/discharge profile of binder-free thick graphene film used as an anode at two different current rates *versus* Li/Li^+ was collected (Fig. 3b and c); the first five cycles were tested at the current rate of 50 mA g^{-1} (Fig. 3b). The long discharge profile observed below 0.2 V corresponded to lithium intercalation into the carbon lattice. The flat discharge and different voltage plateaus indicated that the graphene film was well crystallized, which was also confirmed by Raman and XPS data. The first discharge and charge capacities of the thick graphene film were 448 and 352 mA h g^{-1}, respectively; thus, its coulombic efficiency was calculated to be around 79%. The loss of capacity or irreversible capacity in the first cycle was due to SEI formation, which is characteristic of carbonaceous materials. The SEI formation, a well-known phenomenon of carbon-based electrodes, takes place due to the reduction reaction of electrolyte with the carbon surface at approximately 0.8 V. Furthermore, the same cell was tested at a current rate of 150 mA g^{-1}; all the resulting discharge and charge profiles are shown in Fig. 3c. The discharge and charge capacities were 358 and 350 mA g^{-1}, respectively, corresponding to the very high coulombic efficiency of 97%; this confirmed that there was no further SEI formation during subsequent cycles. Thus the charge/discharge behavior of binder-free thick graphene film showed greater reversible capacity than CNTs grown over Cu and binder-free graphene paper.[28,29] This improvement in

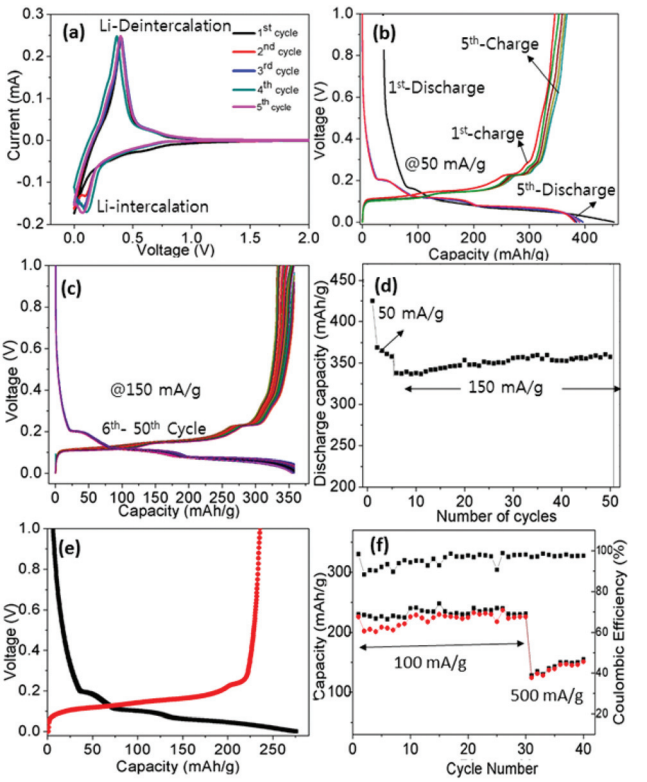

Fig. 3 Electrochemical performance of additive-free thick graphene film (a) cyclic voltammograms in the voltage range of 0–1.5 V with scan rate of 0.5 mV s^{-1}. V up to 5th cycle. Charge and discharge behavior graphene film on Ni in coin cell at different current rates: (b) at 50 mA g^{-1}, (c) at 150 mA g^{-1}. (d) Discharge capacity of the cell with number of cycles at two different current rates up to fifty cycles. (e) First charge and discharge profile of FSG without any additive and current collector, and (f) cyclic performance and coulombic efficiency for 40th cycles at a different current rate (Red and black solid square/circles indicate the charge and discharge capacity, and upper solid squares indicate the coulombic efficiency).

reversible capacity is important when such anode materials are used in full cells which reduces the irreversible capacity to maintain long cycles. The stability of the cell was tested for 50 cycles, and the discharge capacity is plotted as a function of cycle number and is shown in Fig. 3d; the discharge capacity remained almost same even after the 50th cycle, confirming the stability of the cell formed using a thick graphene-based electrode without any additives (binder and conducting agent). After removing Ni, the FSG (without additive and current collector) also used as an anode in a coin half-cell, and charge/discharge profile and cyclic test are shown in Fig. 3(e and f). FSG film after Ni etching could be useful as an anode for flexible LIBs due to its mechanical flexibility, good conductivity and very low weight, which are particularly significant when considering the miniaturization of an energy storage device. Using this idea, we have also tested thick FSG film as the anode in a coin cell *vs.* Li/Li^+. The first charge and discharge profile of FSG are shown in Fig. 3e, which shows the similar characteristic as those based on an anode with Ni current collector (Fig. 3b and c). The first discharge and charge capacity of FSG as anode are calculated to be 250 and 235 mA h g^{-1}, respectively, even though the capacity is lower than that with Ni. However, the reversible capacity is improved in case of FSG. The reason of slightly lower capacity is attributed to the difficulty in measuring exact loading weight, testing the cell at higher current rate and impurities on the surface of FSG during handling. The FSG anode was tested for 40 cycles, and it maintained capacity as almost constant, and a high coulombic efficiency up to 97% was observed, as shown in Fig. 3f.

It is important to test the performance of FSG anodes in full cells before they can be considered suitable for use as materials for flexible LIBs. To test their performance in full cells, we used commercial $LiCoO_2$ as the cathode material and thick graphene films both with Ni and without Ni (FSG) as the anode in coin full-cells; later, the same combination was tested in flexible LIBs. Both cells were tested in the voltage range from 3.0 to 4.2 V with the applied charging and discharging current of 100 μA. The first cycles of the charge and discharge profile of full cells using the graphene films (without additive) with and without Ni are shown in Fig. 4a and b, respectively. The charge and discharge capacities of the full cells with flexible graphene (on Ni) anodes and $LiCoO_2$ cathodes were measured to be around 140 and 115 mA h g^{-1}, respectively; the nearly identical capacities of 140 and 111 mA h g^{-1} were observed in the case of the flexible FSG anode in the full cell. Fig. 4c displayed the rate capability of $LiCoO_2$/FSG cell from 3.0 to 4.2 V at different current rates (0.2, 0.5, 1.0 and 2 C). It can be observed that the cell tested at 0.2 C achieved the highest specific charge and discharge capacity of 133 and 127 mA h g^{-1}, respectively. However, with increasing c-rate, the capacity decreases and becomes minimum at 2 C, which is a common phenomenon as lithium ions do not have enough diffusion time to react with all the particle of cathode material. The first charge/discharge characteristic indicated that the thick graphene film grown over Ni and FSG can serve as a good anode materials as commercial graphite without the use

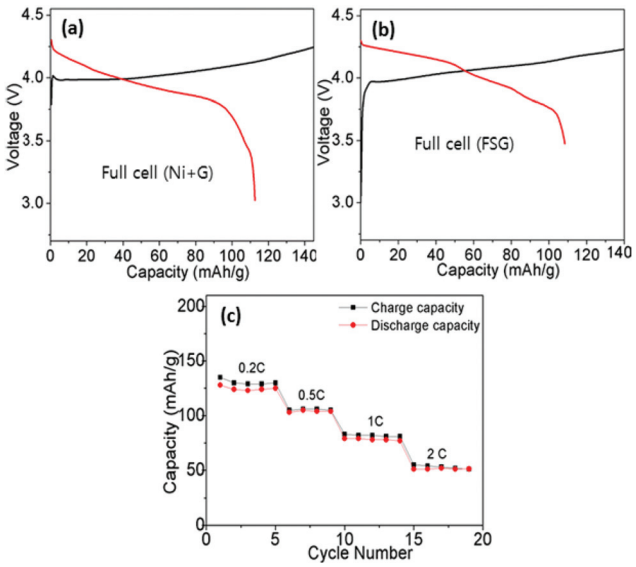

Fig. 4 Charge–discharge behavior of a coin full-cell made with binder-free and freestanding graphene paper using (a) graphene on Ni; (b) after etching Ni freestanding graphene, using $LiCoO_2$ as a cathode in both cases; (c) rate performance of full cell using FSG as an anode *vs.* $LiCoO_2$ cathode.

of any binder, conducting agent or current collector. This will reduce the price, processing complexity and total weight of batteries, as discussed above in the introduction. The thick additive-free flexible graphene film showed good performance as an anode material in both a half and a full coin cell.

Thus, this film is applicable as a flexible anode material for flexible LIBs. Recently, a few articles have been published on flexible LIBs;[6,30,31] however, most of them have been proposed to use either additive (binder) for the electrode materials, or have proposed the use of Li metal as the anode, which has possible safety problems.[16] Therefore, as discussed in the introduction regarding the benefits of binder-free electrode in flexible batteries, we used thick flexible graphene film as a flexible anode and $LiCoO_2$ as the cathode. To make the flexible cathode, we deposited Al thin film (about 400 nm thick) on a plastic (PET) substrate and then coated a thin layer of the cathode over it. Both the cathode and anode were then encapsulated inside a plastic thin film separated with a traditional separator of polypropylene film. Finally, electrolyte was injected inside the plastic encapsulation to complete the flexible battery, which was then tested in both flat and bent states at the current rate of 50 mA g^{-1}.

The battery fabrication process is illustrated schematically in Fig. 1a. The first charge and discharge profiles of the flexible LIB in both the flat and bent state (with the bending radius of about 10 mm) are shown in Fig. 5b. The corresponding strain value of this bending radius (10) mm was calculated around 1%. When FSG is bent with a bending radius up to 5 mm, the corresponding resistance value was observed to be 5Ω, which indicates good mechanical flexibility. The first charge and discharge capacities in the flat state are 135 and

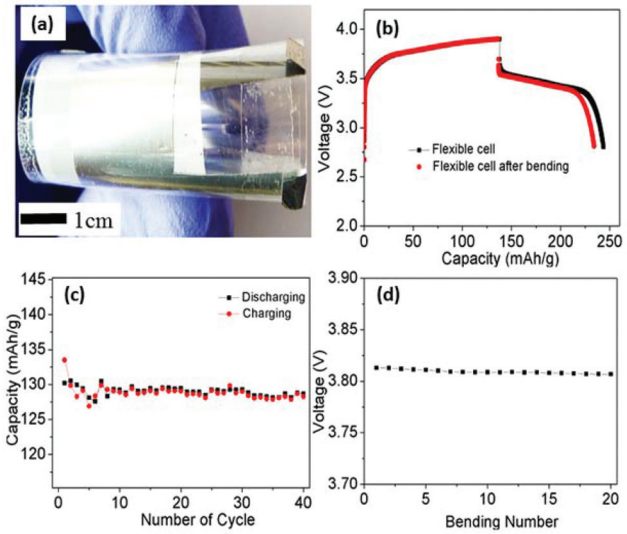

Fig. 5 (a) Camera picture of the flexible lithium ion battery using thick additive-free flexible graphene film as the anode and a $LiCoO_2$ cathode. (b) The first charge and discharge of flexible cell fabricated on plastic substrate in flat and bending state (up to 10 mm). (c) The charge and discharge capacity with number of cycle in bending state. (d) The OCV stability during the number of bending cycle.

110 mA h g^{-1}, respectively. The charge and discharge cycles were measured in the bent state after bending it a number of times with a bending radius of 10 mm. The charge and discharge capacity were estimated to be about 133 and 100 mA h g^{-1}, respectively, thus showing a slight decrease (only 1.2% in charge capacity) in capacity upon bending. Furthermore, the flexible battery was tested for 40 cycles, and the charge and discharge capacity were found to be nearly diminished after repeated cycling, and estimated at approximately 115 mA h g^{-1} (Fig. 5c). The fatigue endurance of the flexible LIB under a number of bending cycles with the bending radius of 10 mm is shown in Fig. 5d. After number of charge/discharge cycling during bending the cell, voltage was measured as an indicator of endurance. The initial cell voltage of the flexible LIB of 3.8 V decreased only slightly to 3.77 V during the repeated bending, showing that anode materials based on the additive-free flexible thick graphene material are promising candidate materials for future flexible electrodes. The advantage of using flexible thick graphene film is that it can be used as a current collector for cathode materials as well.

4. Conclusions

We have synthesized many-layered thick freestanding graphene film by a CVD method and demonstrated that the FSG, which is thin, light weight and a good conductor for electrons and lithium ions, can be successfully used both as anode and anode current collector in coin and flexible cells. The film is suitable for use for LIB applications, and can be used without requiring any metal current collectors, conducting agent or binder. Moreover, high purity and degree of graphitization of a FSG film offers a capacity comparable to that of the graphite anode materials currently used in commercial LIBs. The lithium insertion behavior of thick FSG has been studied in half and full cells, and finally in flexible cells. The additive-free FSG provides high electrical conductivity and chemical stability in both its flat and bent states. This flexible battery could be used to power the flexible electronic devices. This impurity-free flexible structure could also be promising for asymmetric super-capacitor and for a broad range of cathode and anode applications and provides a new design and fabrication route for hybrid materials for a variety of applications. In addition to the electrochemical properties of FSG in the cell, it has few more significant advantages, including (i) direct usability as an electrode without any additive such as conducting agent (carbon black), binder (PVDF) and metal current collector, which are dead cell elements, (ii) simpler fabrication steps than in other carbon nanomaterials, (iii) usability as a current collector for other anode materials and as an anode alone itself and (iv) good mechanical flexibility for electrode of flexible energy storage devices.

Acknowledgements

This work was supported by the Brain Korea (BK) 21 plus program, Research Program (2012R1A2A1A03006049 and 2009-0083540) and the Global Frontier Research Center for Advanced Soft Electronics (2014M3A6A5060933) through the National Research Foundation of Korea (NRF), funded by the Ministry of Education, Science and Technology.

Notes and references

1 M. Winter and R. J. Brodd, *Chem. Rev.*, 2004, **104**, 4245–4269.
2 J. M. Tarascon and M. Armand, *Nature*, 2001, **414**, 359–367.
3 S. Arico, P. Bruce, B. Scrosati, J. M. Tarascon and W. V. Schalkwijk, *Nat. Mater.*, 2005, **4**, 366–377.
4 B. L. Ellis, P. Knauth and T. Djenizian, *Adv. Mater.*, 2014, **26**, 3368–3397.
5 J. B. Goodenough and Y. Kim, *Chem. Mater.*, 2010, **22**, 587–603.
6 L. Hu, H. Wu, F. L. Mantia, Y. Yang and Y. Cui, *ACS Nano*, 2010, **4**, 5843–5848.
7 K. Rana, A. Sil and S. Ray, *Mater. Chem. Phys.*, 2010, **120**, 484–489.
8 B. J. Landi, M. J. Ganter, C. D. Cress, R. A. DiLeo and R. P. Raffaelle, *Energy Environ. Sci.*, 2009, **2**, 638–654.
9 J. Du, S. Pei, L. Ma and H.-M. Cheng, *Adv. Mater.*, 2014, **26**, 1958–1991.
10 E. B. Secor, S. Lim, H. Zhang, C. D. Frisbie, L. F. Francis and M. C. Hersam, *Adv. Mater.*, 2014, **26**, 4533–4538.
11 L. Hu, J. W. Choi, Y. Yang, S. Jeong, F. L. Mantia, L.-F. Cui and Y. Cui, *Proc. Natl. Acad. Sci. U. S. A.*, 2009, **106**, 21490–21494.

12 L. Hu, H. Wu, F. L. Manti, Y. Yang and Y. Cui, *ACS Nano*, 2010, **4**, 5843–5848.
13 S. Luo, K. Wang, J. P. Wang, K. L. Jiang, Q. Q. Li and S. S. Fan, *Adv. Mater.*, 2012, **24**, 2294–2298.
14 H. X. Zhang, C. Feng, Y. C. Zhai, K. L. Jiang, Q. Q. Li and S. S. Fan, *Adv. Mater.*, 2009, **21**, 2299–2304.
15 K. Wang, S. Luo, Y. Wu, X. F. He, F. Zhao, J. P. Wang, K. L. Jiang and S. S. Fan, *Adv. Funct. Mater.*, 2013, **23**, 846–853.
16 M. Koo, K.-Il Park, S. H. Lee, M. Suh, D. Y. Jeon, J. W. Choi, K. Kang and K. J. Lee, *Nano Lett.*, 2012, **12**, 4810–4816.
17 Y. H. Kwon, S.-W. Woo, H.-R. Jung, H. K. Yu, K. Kim, B. H. Oh, S. Ahn, S.-Y. Lee, S.-W. Song, J. Cho, H.-C. Shin and J. Y. Kim, *Adv. Mater.*, 2012, **24**, 5192–5197.
18 W. Weng, H. Lin, X. Chen, J. Ren, Z. Zhang, L. Qiu, G. Guan and H. Peng, *J. Mater. Chem. A*, 2014, **2**, 9306–9312.
19 M. F. El-Kady, V. Strong, S. Dubin and R. B. Kaner, *Science*, 2012, **335**, 1326–1330.
20 J. Shin, K. Park, W.-H. Ryu, J.-W. Jung and I.-D. Kim, *Nanoscale*, 2014, **6**, 12718–12726.
21 W. Sun and Y. Wang, *Nanoscale*, 2014, **6**, 11528–11552.
22 K. Rana, J. Singh, J.-T. Lee, J. H. Park and J.-H. Ahn, *ACS Appl. Mater. Interfaces*, 2014, **6**, 11158–11166.
23 Q. Yu, J. Lian, S. Siriponglert, H. Li, Y. P. Chen and S. S. Pei, *Appl. Phys. Lett.*, 2008, **93**, 113103.
24 A. Dahal and M. Batzil, *Nanoscale*, 2014, **6**, 2548–2562.
25 S.-K. Lee, K. Rana and J.-H. Ahn, *J. Phys. Chem. Lett.*, 2013, **4**, 831–841.
26 G. K. Wertheim, P. M. Van Attekum and S. Basu, *Solid State Commun.*, 1980, **33**, 1127–1130.
27 M. Jean, C. Desnoyer, A. Tranchant and R. Messina, *J. Electrochem. Soc.*, 1995, **142**, 2122–2125.
28 I. Lahiri, S.-W. Oh, J. Y. Hwang, S. Cho, Y.-K. Sun, R. Banerjee and W. Choi, *ACS Nano*, 2010, **4**, 3440–3446.
29 A. Abouimrane, O. C. Compton, K. Amine and S. T. Nguyen, *J. Phys. Chem. C*, 2010, **114**, 12800–12804.
30 N. Li, Z. Chena, W. Ren, F. Li and H.-M. Cheng, *Proc. Natl. Acad. Sci. U. S. A.*, 2012, **109**, 17360–17365.
31 X. Wang, X. Lu, B. Liu, D. Chen, Y. Tong and G. Shen, *Adv. Mater.*, 2014, **26**, 4763–4782.